The Astrophysical Journal, 628:857–866, 2005 August 1

TIME-DEPENDENT NUMERICAL MODEL FOR THE EMISSION OF RADIATION FROM RELATIVISTIC PLASMA

Asaf Pe'er and Eli Waxman
Department of Condensed Matter Physics, Weizmann Institute, Rehovot 76100, Israel; asaf@wicc.weizmann.ac.il
Received 2004 September 22; accepted 2005 March 31

ABSTRACT

We describe a numerical model constructed for the study of the emission of radiation from relativistic plasma under conditions characteristic of, e.g., gamma-ray bursts and active galactic nuclei. The model solves self-consistently the kinetic equations for $e^{\pm}$ and photons, describing cyclosynchrotron emission, direct Compton and inverse Compton scattering, and pair production and annihilation, including the evolution of high-energy electromagnetic cascades. The code allows calculations over a wide range of particle energies, spanning more than 15 orders of magnitude in energy and timescales. Our unique algorithm, which enables to follow the particle distributions over a wide energy range, allows us to accurately derive spectra at high energies, >100 TeV. We present the kinetic equations that are being solved, a detailed description of the equations describing the various physical processes, the solution method, and several examples of numerical results. Excellent agreement with analytical results of the synchrotron–synchrotron self-Compton model is found for parameter-space regions in which this approximation is valid, and several examples are presented of calculations for parameter-space regions for which analytic results are not available.

Subject headings: galaxies: active — gamma rays: bursts — gamma rays: theory — methods: numerical — plasmas — radiation mechanisms: nonthermal

Online material: color figures

1. INTRODUCTION

In the standard fireball scenario of gamma-ray bursts (GRBs), the observable effects are due to the dissipation of kinetic energy in a highly relativistic fireball (see, e.g., Piran 2000; Mészáros 2002; Waxman 2003 for reviews). Synchrotron emission and inverse Compton (IC) emission by accelerated electrons are the main radiative processes. Electrons accelerated in the internal shock waves within the expanding fireball produce the prompt gamma-ray emission, while electrons accelerated in the external shock wave driven by the fireball into the surrounding medium produce the afterglow emission, from the X-ray to the radio bands (Paczyński & Rhoads 1993; Mészáros & Rees 1997; Vietri 1997; Sari et al. 1998; Gruzinov & Waxman 1999).

While being in general agreement with observations (Band et al. 1993; Preece et al. 1998; Frontera et al. 2000; Mészáros 2002), both theoretical arguments and observational evidence suggest that the optically thin synchrotron–synchrotron self-Compton (SSC) emission model is not complete in explaining either the prompt or the afterglow emission. Additional physical processes can significantly modify the SSC spectrum. First, over a wide range of model parameters, a large number of $e^{\pm}$ pairs are produced in internal collisions, due to annihilation of high-energy photons. Second, relativistic pairs cool rapidly to mildly relativistic energy, where their energy distribution is determined by a balance between emission and absorption of radiation. The emergent spectrum, which is affected by scattering off the pair population, depends strongly on the pair energy distribution, and in particular on the "effective temperature" that characterizes the low-end of the energy distribution. Third, proton and electron acceleration to high energies initiates rapid electromagnetic cascades. It is necessary to follow the evolution of a high-energy, nonlinear cascade in order to accurately derive the spectrum. And last, the plasma is not in steady state, and the particle distributions are continuously evolving.

On the observational side, we note that hard spectra, $\nu F_{\nu} \propto \nu^{\alpha}$ with $\alpha > 4/3$ at low energies, $\lesssim$300 keV, were observed at early times in some GRBs (Preece et al. 1998; Frontera et al. 2000; Ghirlanda et al. 2003). These hard spectra are inconsistent with the optically thin synchrotron–SSC model predictions. A similar conclusion was obtained by a comparison of the high-energy and low-energy spectral indices during the prompt emission phase of 150 GRBs (Preece et al. 2002). An additional high-energy (>1 MeV) spectral component inconsistent with the synchrotron model prediction was reported by González et al. (2003). Finally, a recent analysis by Baring & Braby (2004) showed difficulty in explaining the high-energy component of GRBs' early emission by the SSC model.

The above-mentioned difficulties raise the need for a model that can better describe emission under conditions characterizing GRBs. However, a numeric calculation of GRB spectra that takes into consideration creation and annihilation of pairs is complicated. The evolution of electromagnetic cascades initiated by the annihilation of high-energy photons occurs on a very short timescale. On the other extreme, evolution of the low-energy, mildly relativistic pairs, which is governed by synchrotron self-absorption and direct and inverse Compton emission, takes much longer. The large difference in characteristic timescales poses a challenge to numeric calculations. Another challenge to numerical modeling is due to the fact that at mildly relativistic energies the usual synchrotron emission and IC scattering approximations are not valid, and precise cyclosynchrotron emission and direct Compton and inverse Compton scattering calculations are required.

Two approaches have been employed so far in treating this problem. The first is the Monte Carlo approach, in which individual particles are followed as they undergo interactions inside the plasma. This scheme typically suffers from relatively poor photon statistics at high energies and does not lend itself to time-dependent calculations. Work done so far using this approach

(Pilla & Loeb 1998) was limited to parameter-space regions where the creation of pairs has only a minor effect on the resulting spectrum. The second approach involves solving the relevant kinetic equations. Following the time evolution of the system by using this method is straightforward, and photon statistics at high energies is not an issue. However, the above-mentioned complications limit the accuracy of the numerical models constructed so far (Panaitescu & Mészáros 1998) above $\sim$1 GeV.

Note that this method was extensively used in the past in the study of active galactic nucleus (AGN) plasma (Zdziarski & Lightman 1985; Fabian et al. 1986; Lightman & Zdziarski 1987; Coppi 1992). Using the numerical models, new results were obtained, such as the effective pair temperature and the complex pattern of the spectral indices in the X-ray (2–10 keV) range (Lightman & Zdziarski 1987), that were not obtained by previous analytic calculations. None of these models, however, considered the evolution of high-energy electromagnetic cascades expected to be relevant for both GRBs and AGNs. In addition, the treatment of photon emission in the presence of magnetic field was not complete, since particles are expected to accumulate at low energies ($\gamma \sim 1$), where the synchrotron emission approximation used does not hold, and exact treatment of cyclosynchrotron emission is required.

Pair cascade evolution was first studied by Bonometto & Rees (1971). Small-angle cascade showers in anisotropic radiation fields were treated by Burns & Lovelace (1982). Guilbert et al. (1983) and Svensson (1987) have generalized the treatment of cascade evolution, showing that it may have a significant effect on the high-energy spectrum. It is therefore necessary to incorporate the cascade calculation in order to accurately derive the high-energy emission spectrum.

We have constructed a numerical model that overcomes the numerical challenges. Applying this model to GRB plasmas, we have obtained several new results. For example, we have shown (Pe'er & Waxman 2004b) that emission peaks at $\sim$1 MeV for $\tau_{\pm} \sim 10-10^2$, where $\tau_{\pm}$ is the optical depth to scattering by pairs, and that peak energy at $\gg$MeV cannot be obtained for GRB luminosity $L \sim 10^{52}$ ergs s^{-1}. We showed that for large compactness, $l' > 100$, the spectral slope below 1 MeV is steep, $\varepsilon^2 n_{\rm ph}(\varepsilon) \propto \epsilon^{\alpha}$ with $0.5 < \alpha < 1$, and shows a sharp cutoff at 10 MeV. We also showed (Pe'er & Waxman 2004c) that observations of the early afterglow emission at 1 GeV to 1 TeV is informative about two of the most poorly determined parameters of the fireball model: the ambient matter density and the fraction of thermal energy carried by the magnetic field, ϵ_B.

We present in this paper our numerical model. In § 2 we describe the basic model assumptions. We then present the kinetic equations that are being solved and detailed description of the numerical treatment of various physical processes. Our numerical integration approach is described in § 3. We present the general approach of treating this complicated problem, and the various integration techniques used. In § 4 we give examples of numerical results, relevant to the prompt emission phase of GRBs, and compare them to approximate analytic results. We summarize in § 5 the main features of our method and discuss its usefulness for the ongoing research of GRBs and AGNs.

2. MODEL ASSUMPTIONS AND PHYSICAL PROCESSES

We consider a uniform plasma, composed of protons, electrons, positrons, and photons, and permeated by a time-independent magnetic field. The particle and photon distributions are assumed homogeneous and isotropic. Considering the physical phenomenon of, e.g., GRB as a motivation, these assumptions are equivalent to the assumption that the calculations are carried out in the comoving frame (see § 4 below). We assume the existence of a dissipation process (e.g., collisionless shock waves) that produces energetic particles at constant rates, $Q(\gamma)$ and $S(\gamma)$ for electrons and protons, respectively, per unit time per unit volume per unit Lorentz factor γ. Since the details of the acceleration process are not yet known, we do not specify here the functions $Q(\gamma)$ and $S(\gamma)$. These functions are specified when treating a particular problem (see § 4). Motivated by the GRB fireball model scenario in which the internal shock waves cross the colliding shells at relativistic speeds, we assume that the dissipation process occurs on a characteristic timescale that is equal to the light crossing time, $t_{\rm dyn} \sim R/c$, where R is a characteristic length scale of the plasma.

The population of electrons, positrons, and photons is affected by synchrotron emission, synchrotron self-absorption, Compton scattering, pair production, and pair annihilation, which occur simultaneously during the dynamical time $t_{\rm dyn}$. In this version of the code, protons are assumed to interact via photomeson interactions only, producing pions that decay into energetic photons and positrons. Coulomb scattering is not considered, because, as we show in the Appendix, it is insignificant in calculating the spectra under conditions that are of interest to us. As noted by Coppi & Blandford (1990), *e-e* bremsstrahlung is also insignificant under the same conditions and is therefore not included in the calculations.

We assume no photon escape during the dynamical time $t_{\rm dyn}$ and instantaneous photon release at the end of the dynamical time. This approximation is justified since the dynamical time is equal to the light crossing time. If $\tau_{\rm T}$, the optical depth to Thomson scattering by electrons or by the created pairs at the end of the dynamical time, is larger than 1, the "instantaneous release" approximation is not valid. Since the plasma is assumed to be heated to relativistic energy density, we assume in this case that the dissipation phase is followed by a relativistic expansion phase, during which the optical depth decreases. The evolution of particle and photon distributions is followed during the expansion phase until the optical depth for Thomson scattering, $\tau_{\rm T} < 1$. A detailed description of this calculation is given in Pe'er & Waxman (2004b).

Let $n_{e^-}(\gamma, t)$, $n_{e^+}(\gamma, t)$, and $n_p(\gamma, t)$ be the number density per unit Lorentz factor γ, per unit volume of electrons, positrons, and protons, and let $n_{\rm ph}(\varepsilon, t)$ be the number density per unit energy per unit volume of photons. The time derivatives of the electron, positron, proton, and photon number densities are given by

$$\frac{\partial n_{e^-}(\gamma,t)}{\partial t} = Q(\gamma) + \frac{\partial}{\partial \gamma}\left\{ n_{e^-}(\gamma,t)[P_S(\gamma) + P_C(\gamma,t)] + H(\gamma,t)\beta\gamma^2 \frac{\partial}{\partial \gamma}\left[\frac{n_{e^-}(\gamma,t)}{\beta\gamma^2}\right]\right\} + \frac{\partial n_{eP}(\gamma,t)}{\partial t} - \frac{\partial n_{eA}(\gamma,t)}{\partial t}, \quad (1)$$

$$\frac{\partial n_{e^+}(\gamma,t)}{\partial t} = \frac{\partial}{\partial \gamma}\left\{ n_{e^+}(\gamma,t)[P_S(\gamma) + P_C(\gamma,t)] + H(\gamma,t)\beta\gamma^2 \frac{\partial}{\partial \gamma}\left[\frac{n_{e^+}(\gamma,t)}{\beta\gamma^2}\right]\right\} + \frac{\partial n_{eP}(\gamma,t)}{\partial t} - \frac{\partial n_{eA}(\gamma,t)}{\partial t} + Q_{\pi}(\gamma,t), \quad (2)$$

$$\frac{\partial n_p(\gamma,t)}{\partial t} = S(\gamma) + \frac{\partial}{\partial \gamma}\left[n_p(\gamma,t)P_{\pi}(\gamma,t)\right], \quad (3)$$

$$\frac{\partial n_{ph}(\varepsilon,t)}{\partial t} = R_S(\varepsilon,t) + R_C(\varepsilon,t) - R_P(\varepsilon,t) + R_A(\varepsilon,t) + R_\pi(\varepsilon,t) - cn_{\rm ph}(\varepsilon,t)\alpha(\varepsilon,t). \quad (4)$$

Here the terms in the curly brackets on the right-hand side of equations (1) and (2) give the change of population due to synchrotron emission and Compton scattering; $P_S(\gamma)$ and $P_C(\gamma,t)$ are the synchrotron and Compton emitted power. The third term in the curly brackets represents energy gain by synchrotron self-absorption, with $H(\gamma,t)$ defined below (see eq. [5]). The last two terms in equation (1), $\partial n_{eP}(\gamma,t)/\partial t$ and $\partial n_{eA}(\gamma,t)/\partial t$, are the rates of pair creation and pair annihilation per unit volume. The term $Q_\pi(\gamma,t)$ in equation (2) represents positron creation by the decay of π^+. The pions are produced by photomeson interactions of low-energy photons with energetic protons. In the proton equation, $P_\pi(\gamma,t)$ is the rate of proton energy transfer to pions. In the photon equation, $R_S(\varepsilon,t)$, $R_C(\varepsilon,t)$, $R_P(\varepsilon,t)$, and $R_A(\varepsilon,t)$ are the rate of production and annihilation of photons due to synchrotron emission, Compton scattering, pair production, and pair annihilation, and $R_\pi(\varepsilon,t)$ is the production rate of photons due to the decay of energetic pions. The last term represents photon reabsorption, where $\alpha(\varepsilon,t)$ is the self-absorption coefficient.

In the rest of this section, we present a detailed description of the terms in equations (1)–(4).

2.1. *Synchrotron and Synchrotron Self-Absorption Emission Terms*

The term $H(\gamma,t)$ in equation (1) describes the heating of the electrons and their diffusion in energy due to synchrotron self-absorption. It is given by

$$H(\gamma,t) = \int d\omega \frac{I_\omega(t)}{4\pi m_e\omega^2} P(\omega,\gamma) \quad (5)$$

(see McCray 1969; Ginzburg & Syrovatskii 1969; Ghisellini et al. 1988). The specific intensity $I_\omega(t)$ is calculated using $I_\omega(t) = n_{\rm ph}(\varepsilon,t)\varepsilon c\hbar/4\pi$, where $\varepsilon = \hbar\omega$; $P(\omega,\gamma)$ is the total power emitted by an electron having Lorentz factor γ per unit frequency ω and is given in § 2.1.1.

The time derivative of photon distribution due to synchrotron emission is given by

$$R_S(\varepsilon,t) = \frac{1}{\hbar}\int d\gamma P(\omega,\gamma) n_{e^\pm}(\gamma,t), \quad (6)$$

where $n_{e^\pm}(\gamma,t) \equiv n_{e^-}(\gamma,t) + n_{e^+}(\gamma,t)$.

In a homogeneous plasma, the self-absorption coefficient is given by

$$\alpha(\varepsilon,t) = -\frac{\pi^2}{8m_e\omega^2}\int d\gamma P(\omega,\gamma)\beta\gamma^2 \frac{\partial}{\partial\gamma}\left[\frac{n_{e^\pm}(\gamma,t)}{\beta\gamma^2}\right] \quad (7)$$

(Ginzburg & Syrovatskii 1969; Rybicki & Lightman 1979).

2.1.1. *Cyclosynchrotron Emission Spectrum*

The power (energy/time/sr/frequency) emitted by a single electron moving with velocity $\beta \equiv v/c$ in a frequency range ω to $\omega + d\omega$ at an angle θ with respect to the magnetic field is given by

$$\eta_\omega(\beta,\theta)d\omega = \frac{q^2\omega^2}{2\pi c}\left[\sum_{m=1}^{\infty}\left(\frac{\cos\theta - \beta_\parallel}{\sin\theta}\right)^2 J_m^2(x) + \beta_\perp^2 J_m'^2(x)\right]\delta(y)d\omega \quad (8)$$

(see Bekefi 1966; Ginzburg & Syrovatskii 1969; Mahadevan et al. 1996). Here

$$x = \frac{\omega}{\omega_0}\beta_\perp \sin\theta, \quad (9)$$

$$\omega_0 = \frac{\omega_b}{\gamma}, \quad \omega_b \equiv \frac{qB}{m_e c}, \quad (10)$$

$$y = m\omega_0 - \omega(1 - \beta_\parallel\cos\theta); \quad (11)$$

$J_m(x)$ is the Bessel function of order m, $J_m'(x)$ is its derivative, $\beta_\parallel = \beta\cos\theta_p$ and $\beta_\perp = \beta\sin\theta_p$ are the velocity components parallel and perpendicular to the magnetic field, and θ_p is the angle between the electron velocity direction and the magnetic field. The presence of a δ-function implies that the emission occurs at discrete frequencies.

The total power emitted by a single electron having Lorentz factor $\gamma \equiv (1-\beta^2)^{-1/2}$ per unit frequency ω is given by integrating $\eta_\omega(\beta,\theta)$ over the solid angle $d\Omega \equiv \sin\theta\, d\theta\, d\phi$. For an isotropic distribution of electrons, the mean radiated power is given by

$$P(\omega,\gamma) \equiv \frac{dE}{dt\, d\omega} = \frac{2}{4\pi}\int_0^{2\pi} d\phi_p \int_0^1 d(\cos\theta_p)\int_0^{2\pi} d\phi \int_{-1}^1 d(\cos\theta)\eta_\omega(\beta,\theta) = 2\pi\int_0^1 d(\cos\theta_p)\int_{-1}^1 d(\cos\theta)\eta_\omega(\beta,\theta), \quad (12)$$

where the factor of $1/4\pi$ comes from angular normalization of the isotropic distribution, and the factor of 2 is due to integration on half of the range of $\cos\theta_p$.

In the synchrotron limit $\gamma \gg 1$, the Bessel functions can be approximated by modified Bessel functions, resulting in the well-known result

$$P(\omega,\gamma) = \frac{\sqrt{3}q^3 B\sin\theta_p}{2\pi m_e c^2} F(X), \quad (13)$$

where

$$X = \frac{\omega}{\omega_c}, \quad \omega_c = \frac{3}{2}\gamma^2\frac{qB}{m_e c}\sin\theta_p; \quad (14)$$

$F(X)$ is given by

$$F(X) \equiv X\int_X^\infty K_{5/3}(\xi)d\xi, \quad (15)$$

where $K_{5/3}(\xi)$ is modified Bessel function. The function $F(X)$ was tabulated in, e.g., Ginzburg & Syrovatskii (1965).

The power emitted by a single electron is given by integrating equations (12) and (13) over all frequencies,

$$P_S(\gamma) \equiv \int P(\omega,\gamma)d\omega = \frac{2q^4B^2\gamma^2\beta^2\sin^2\theta_p}{3m_e^2c^3} \qquad (16)$$

(see, e.g., Rybicki & Lightman 1979).

The calculation method of the cyclosynchrotron emission spectrum $P(\omega,\gamma)$ is determined by the electron energy: (1) For low-energy electrons having $\gamma < 3.2$ ($\beta < 0.95$), integration of equation (12) is carried out explicitly at all frequencies up to $\omega/\omega_b = 200$. Above this frequency, no emission is assumed. (2) For electrons with $3.2 < \gamma < 10$, equation (12) is solved up to $\omega/\omega_b = 100$. Above this frequency, the approximate synchrotron spectrum (eq. [13]) is calculated up to $\omega \le 10\omega_c$. (3) At high electron energies, $\gamma > 10$, the synchrotron spectrum (eq. [13]) is calculated in the range $0.001\omega_c < \omega < 10\omega_c$.

2.2. *Compton Scattering*

The total power emitted by Compton scattering by a single electron having Lorentz factor γ into a unit volume is given by

$$P_C(\gamma,t) = \int d\alpha_1 \int d\alpha \frac{d^2N(\gamma,\alpha_1)}{dt\,d\alpha} n_{\rm ph}(\alpha_1,t)(\alpha-\alpha_1), \quad (17)$$

where $d^2N(\gamma,\alpha_1)/dt\,d\alpha$ is the rate of scattering by a single electron having Lorentz factor γ passing through space filled with a unit density (1 photon per unit volume) of isotropically distributed, monoenergetic photons with energy $\alpha_1 m_e c^2$. Note that the Compton power can be negative (i.e., the electron gains energy), depending on the initial photon number density distribution $n_{\rm ph}(\alpha_1,t)$.

The time evolution of the photon number density due to Compton scattering is given by

$$R_C(\alpha,t) = \int d\gamma n_{e^\pm}(\gamma,t) \int d\alpha_1 n_{\rm ph}(\alpha_1,t) \times \left[\frac{d^2N(\gamma,\alpha_1)}{dt\,d\alpha} - \frac{d^2N(\gamma,\alpha)}{dt\,d\alpha_1}\right]. \qquad (18)$$

2.2.1. *Compton Scattering Spectrum*

The rate of scattering by a single electron having Lorentz factor γ passing through space filled with a unit density of isotropically distributed, monoenergetic photons with energy $\alpha_1 m_e c^2$ was first derived by Jones (1968),

$$\frac{d^2N(\gamma,\alpha_1)}{dt\,d\alpha} = \frac{\pi r_0^2 c\alpha}{2\gamma^4\beta\alpha_1^2}[F(\zeta_+) - F(\zeta_-)]. \qquad (19)$$

Here α is the energy of the outgoing photon in units of $m_e c^2$, r_0 is the classical electron radius, $\beta = (1-1/\gamma^2)^{1/2}$, $\zeta_\pm$ are the upper and lower integration limits (see below), and $F(\zeta)$ is given by the sum of 12 functions obtained by solving equation (21) of Jones (1968).[1]

[1] Note that in eq. (21) of Jones, there is a misprint by a factor of a in the penultimate term. Note, though, that the claim of Coppi & Blandford (1990) regarding an error in eq. (20) of Jones (1968) is incorrect. In fact, eq. (A1.1) of Coppi & Blandford (1990) is identical to eq. (20) of Jones (1968).

Solving equation (21) of Jones (1968), $F(\zeta)$ is given by

$$F(\zeta) = \sum_{i=1}^{12} f_i,$$

$$f_1 = \left(\frac{\gamma}{\alpha}\right)^2\left(\frac{\gamma}{\alpha_1}\right)\sqrt{E_1},$$

$$f_2 = -\left(\frac{\gamma}{\alpha}\right)\frac{2}{\sqrt{a}}\log\left(\frac{\sqrt{a}+\sqrt{E_1}}{\sqrt{b\zeta}}\right),$$

$$f_3 = -\frac{\sqrt{E_1}}{a\zeta} - \frac{\alpha_1}{\gamma}\frac{2}{a^{3/2}}\log\left(\frac{\sqrt{a}+\sqrt{E_1}}{\sqrt{b\zeta}}\right),$$

$$f_4 = -\left(\frac{\gamma}{\alpha}\right)^2\left(\frac{\alpha_1}{\gamma}+1\right)\left(\frac{\alpha}{\alpha_1}+1\right)\frac{1}{\sqrt{E_1}},$$

$$f_5 = \left(\frac{\gamma}{\alpha}\right)^2\frac{\gamma}{2\alpha_1}\left(\sqrt{E_1}+\frac{a}{\sqrt{E_1}}\right),$$

$$f_6 = \left(\frac{\gamma}{\alpha}\right)\left(\frac{\alpha_1}{\gamma}+1\right)^2\frac{2}{a\sqrt{E_1}} - 2\left(\frac{\gamma}{\alpha}\right)\frac{(\alpha_1/\gamma+1)^2}{a^{3/2}}\log\left(\frac{\sqrt{a}+\sqrt{E_1}}{\sqrt{b\zeta}}\right),$$

$$f_7 = -4\left(\frac{\gamma}{\alpha}\right)\frac{\gamma}{\sqrt{|c|}}\begin{cases}\sinh^{-1}\left(\sqrt{\dfrac{c\zeta}{d}}\right) & c>0,\\ \sin^{-1}\left(\sqrt{-\dfrac{c\zeta}{d}}\right) & c<0,\end{cases}$$

$$f_8 = \left(\frac{\gamma}{\alpha}\right)^2\gamma\frac{\sqrt{E_2}}{c} - \left(\frac{\gamma}{\alpha}\right)^2 d\frac{\gamma}{|c|^{3/2}} \times \begin{cases}\sinh^{-1}\left(\sqrt{\dfrac{c\zeta}{d}}\right) & c>0,\\ (-1)\sin^{-1}\left(\sqrt{-\dfrac{c\zeta}{d}}\right) & c<0,\end{cases}$$

$$f_9 = -\frac{2\gamma}{d}\frac{\sqrt{E_2}}{\zeta},$$

$$f_{10} = \frac{4\alpha c\zeta}{d^2\sqrt{E_2}} + \frac{2\alpha}{d\sqrt{E_2}},$$

$$f_{11} = \alpha\gamma^2\left(\frac{\alpha_1}{\gamma} - \frac{\alpha}{\gamma} + 1 + \frac{\alpha_1}{\alpha}\right)\frac{2\zeta}{d\sqrt{E_2}},$$

$$f_{12} = \alpha_1\gamma^2\frac{2\zeta}{c\sqrt{E_2}} - \alpha_1\gamma^2\frac{2}{|c|^{3/2}}\begin{cases}\sinh^{-1}\left(\sqrt{\dfrac{c\zeta}{d}}\right) & c>0,\\ (-1)\sin^{-1}\left(\sqrt{-\dfrac{c\zeta}{d}}\right) & c<0.\end{cases} \qquad (20)$$

Here

$$a = 1\Big/\gamma^2\Big[(\alpha_1+\gamma)^2-1\Big],$$
$$b = 2\alpha_1/\gamma,$$
$$c = (\gamma-\alpha)^2 - 1,$$
$$d = 2\alpha/\gamma,$$
$$E_1 = a - b\zeta,$$
$$E_2 = c\zeta^2 + d\zeta. \qquad (21)$$

The integration limits depend on the energy of the outgoing photon, α, best presented as a function of the parameter $\rho \equiv \alpha/\alpha_1$. The minimum value of ρ is[2]

$$\rho_{\min} = \frac{1-\beta}{1+\beta+2\alpha_1/\gamma}, \tag{22}$$

while the upper value of ρ is limited by the kinematics,

$$\rho_{\max,1} = 1 + (\gamma - 1)/\alpha_1, \tag{23}$$

and by the requirement that $\zeta \le 1+\beta$,

$$\rho_{\max,2} = \frac{1+\alpha_1/\gamma+\sqrt{(1+\alpha_1/\gamma)^2-1+\beta^2-2\alpha_1/\gamma(1+\beta)}}{1-\beta+2\alpha_1/\gamma}, \tag{24}$$

resulting in $\rho_{\max} = \min(\rho_{\max,1},\ \rho_{\max,2})$.

For a given ρ, $\rho_{\min} \le \rho \le \rho_{\max}$, the integration boundaries are

$$\zeta_-(\rho) = \max\left(\rho\left\{\left(1+\frac{\alpha_1}{\gamma}-\frac{\rho\alpha_1}{\gamma}\right) - \left[\left(1+\frac{\alpha_1}{\gamma}-\frac{\rho\alpha_1}{\gamma}\right)^2 - \frac{1}{\gamma^2}\right]^{1/2}\right\},\ 1-\beta\right) \tag{25}$$

and

$$\zeta_+(\rho) = \min\left(\rho\left\{\left(1+\frac{\alpha_1}{\gamma}-\frac{\rho\alpha_1}{\gamma}\right) + \left[\left(1+\frac{\alpha_1}{\gamma}-\frac{\rho\alpha_1}{\gamma}\right)^2 - \frac{1}{\gamma^2}\right]^{1/2}\right\},\ 1+\beta\right). \tag{26}$$

For an energetic electron, $\gamma \gg 1$ and $\gamma \gg \alpha_1$, equation (19) can be simplified and the scattering rate is given by (Jones 1968; Blumenthal & Gould 1970)

$$\frac{d^2N(\gamma,\alpha_1)}{dt\,d\alpha} \approx \frac{2\pi r_0^2 c}{\alpha_1\gamma^2}\left[2q\log q + (1+2q)(1-q) + \frac{1}{2}\frac{(4\alpha_1\gamma q)^2}{(1+4\alpha_1\gamma q)}(1-q)\right], \tag{27}$$

where $q \equiv \alpha/4\alpha_1\gamma^2(1-\alpha/\gamma)$ is limited to $1/4\gamma^2 < q \le 1$.

Calculation of the spectrum resulting from Compton scattering is determined by the electron Lorentz factor γ and the incoming photon energy, α_1. (1) For $\gamma > 10^4$ and $\alpha_1 < 10^{-5}$, the approximate spectrum (eq. [27]) is used. (2) For all other values of γ, α_1, the exact spectrum (eq. [19]) is calculated. The results are tabulated in a three-dimensional matrix (initial electron energy × initial photon energy × final photon energy) and are used in calculating the time derivatives of electron and photon number densities.

2.3. *Pair Production*

The production rate of particles having Lorentz factor in the range γ to $\gamma + d\gamma$ by an isotropic photon field with photon density $n_{\rm ph}(\alpha,t)$ was calculated by Bötcher & Schlickeiser (1997),

$$\frac{\partial n_{eP}(\gamma,t)}{\partial t} = \frac{3}{4}\sigma_{\rm T} c \int_0^\infty d\alpha_1 \frac{n_{\rm ph}(\alpha_1,t)}{\alpha_1^2}\int_{\max(1/\alpha_1,\,\gamma+1-\alpha_1)}^\infty d\alpha_2 \frac{n_{\rm ph}(\alpha_2,t)}{\alpha_2^2} \times \left(\frac{\sqrt{E^2-4\alpha_{\rm cm}^2}}{4} + H_+ + H_-\right)\Bigg|_{\alpha_{\rm cm}^L}^{\alpha_{\rm cm}^U}; \tag{28}$$

$\alpha_{1,2}$ are the scattering photons energies in units of $m_e c^2$, $E = \alpha_1 + \alpha_2$, and $\alpha_{\rm cm}$ is the photon energy in the center-of-momentum frame, given by $2\alpha_{\rm cm}^2 = \alpha_1\alpha_2$. The functions $H_\pm$ are calculated using

$$c_\pm \equiv (\alpha_{1,2} - \gamma)^2 - 1, \tag{29}$$

$$d_\pm \equiv \alpha_{1,2}^2 + \alpha_1\alpha_2 \pm \gamma(\alpha_2 - \alpha_1). \tag{30}$$

For $c_\pm \ne 0$, $H_\pm$ are given by

$$H_\pm = -\frac{\alpha_{\rm cm}}{8\sqrt{\alpha_1\alpha_2 + c_\pm\alpha_{\rm cm}^2}}\left(\frac{d_\pm}{\alpha_1\alpha_2}+\frac{2}{c_\pm}\right) + \frac{1}{4}\left(2 - \frac{\alpha_1\alpha_2 - 1}{c_\pm}\right)I_\pm + \frac{\sqrt{\alpha_1\alpha_2 + c_\pm\alpha_{\rm cm}^2}}{4}\left(\frac{\alpha_{\rm cm}}{c_\pm} + \frac{1}{\alpha_{\rm cm}\alpha_1\alpha_2}\right), \tag{31}$$

where

$$I_\pm = \begin{cases} \dfrac{1}{\sqrt{c_\pm}}\ln\left(\alpha_{\rm cm}\sqrt{c_\pm} + \sqrt{\alpha_1\alpha_2 + c_\pm\alpha_{\rm cm}^2}\right) & c_\pm > 0, \\ \dfrac{1}{\sqrt{-c_\pm}}\arcsin\left(\alpha_{\rm cm}\sqrt{-\dfrac{c_\pm}{\alpha_1\alpha_2}}\right) & c_\pm < 0. \end{cases} \tag{32}$$

For $c_\pm = 0$,

$$H_\pm = \left(\frac{\alpha_{\rm cm}^3}{12} - \frac{\alpha_{\rm cm} d_\pm}{8}\right)\frac{1}{(\alpha_1\alpha_2)^{3/2}} + \left(\frac{\alpha_{\rm cm}^3}{6} + \frac{\alpha_{\rm cm}}{2} + \frac{1}{4\alpha_{\rm cm}}\right)\frac{1}{\sqrt{\alpha_1\alpha_2}}. \tag{33}$$

The upper and lower integration limits $\alpha_{\rm cm}^U$, $\alpha_{\rm cm}^d$ are given by

$$\alpha_{\rm cm}^U = \min\left(\sqrt{\alpha_1\alpha_2},\ \alpha_{\rm cm}^a\right), \quad \alpha_{\rm cm}^L = \max\left(1,\ \alpha_{\rm cm}^b\right), \tag{34}$$

where

$$\left(\alpha_{\rm cm}^{a,b}\right)^2 = \frac{1}{2}\left\{\gamma(E-\gamma) + 1 \pm \sqrt{[\gamma(E-\gamma)+1]^2 - E^2}\right\}. \tag{35}$$

The total loss rate of photons in the energy range α_1 to $\alpha_1 + d\alpha_1$ by pair production is given by

$$R_P(\alpha_1,t) = -n_{\rm ph}(\alpha_1,t)\frac{c}{2} \times \int d(\cos\theta)(1-\cos\theta)\int_{2/\alpha_1(1-\cos\theta)}^\infty d\alpha_2 n_{\rm ph}(\alpha_2,t)\sigma(\alpha_1,\alpha_2,\theta), \tag{36}$$

[2] Note that there is a misprint in the result that appears in Jones (1968).

where

$$\sigma(\alpha_1,\alpha_2,\theta)= \frac{3}{16}\sigma_{\rm T}(1-\beta'^2)\left[2\beta'(\beta'^2-2)+(3-\beta'^4)\ln\left(\frac{1+\beta'}{1-\beta'}\right)\right] \quad (37)$$

and

$$\beta'=\left[1-\frac{2}{\alpha_1\alpha_2(1-\cos\theta)}\right]^{1/2} \quad (38)$$

(Gould & Schréder 1967; Lang 1999). The resulting particle spectra are symmetric for electrons and positrons.

Calculation of the photon loss rate is carried out using equation (36). The spectra of the emergent pairs is calculated in accordance to the photon energies: (1) For $1.001 \le \alpha_1\alpha_2 \le 10^4$, equation (28) is solved and the exact spectrum is obtained. (2) For $\alpha_1\alpha_2 < 1.001$, a monoenergetic spectrum of the created particles assumed, with energy $(\alpha_1+\alpha_2)/2$. (3) If $\alpha_1\alpha_2 > 10^4$, the energy of one of the created particles is taken to be $\alpha_{\rm max} \equiv \max(\alpha_1,\alpha_2)$, and for the second particle the energy is approximated as $\alpha_{\rm min}+1/(2\alpha_{\rm min})$, where $\alpha_{\rm min}\equiv\min(\alpha_1,\alpha_2)$.

2.4. *Pair Annihilation*

The total loss rate of electrons having Lorentz factor γ_1 to $\gamma_1+d\gamma_1$ due to pair production (in the plasma frame) is given by

$$\frac{\partial n_{e^-A}(\gamma_1,t)}{\partial t}=-n_{e^-}(\gamma_1,t)\frac{c}{2\gamma_1} \times\int d(\cos\theta)\int d\gamma_2 n_{e^+}(\gamma_2,t)\beta_2'\frac{dn'}{dn}\sigma_{\rm ann}(\gamma_2'), \quad (39)$$

where $\gamma_2'=\gamma_1\gamma_2(1+\beta_1\beta_2\cos\theta)$ is the positron Lorentz factor in the electron's rest frame, β_2' is its velocity in this frame, and $dn'/dn=\gamma_1(1+\beta_1\beta_2\cos\theta)$. The cross section for a positron having Lorentz factor γ to annihilate with an electron at rest, $\sigma_{\rm ann}(\gamma)$, is given by

$$\sigma_{\rm ann}(\gamma)=\frac{3}{8}\frac{\sigma_{\rm T}}{\gamma+1}\left[\frac{\gamma^2+4\gamma+1}{\gamma^2-1}\ln\left(\gamma+\sqrt{\gamma^2-1}\right)-\frac{\gamma+2}{\sqrt{\gamma^2-1}}\right] \quad (40)$$

(Svensson 1982; Lang 1999). The loss rate of positrons is calculated in a similar way.

The annihilation rate is calculated by solving equation (39). Since (1) it was shown in Svensson (1982) that for a large region of γ_1, γ_2 the photon spectrum is narrowly peaked around $\varepsilon_{1,2}=\gamma_{1,2}m_ec^2$, and since (2) we found numerically that calculation of the exact particle spectrum resulting after pair production, compared to the approximate particle spectrum $\gamma_{1,2}=\varepsilon_{1,2}/m_ec^2$, did not have a significant effect on the resulting photon spectra, we decided not to include calculation of the pair-annihilated photon spectra in this version of the code. The emergent photon energies are assumed to be equal to the reacting particle energies, $\varepsilon_{1,2}=\gamma_{1,2}m_ec^2$; thus

$$R_A(\epsilon=\gamma m_ec^2,\ t)=-\frac{dn_{eA}(\gamma,t)}{dt}. \quad (41)$$

2.5. *Photon and Positron Production by π Decay*

Photomeson interactions between energetic protons and low-energy photons result in production of pions. The fractional energy loss rate of a proton with Lorentz factor γ_p due to pion production is

$$t_\pi^{-1}(\gamma_p,t)\equiv-\frac{1}{\gamma_p}\frac{d\gamma_p}{dt} =\frac{1}{2\gamma_p^2}c\int_{\varepsilon_0}^{\infty}d\varepsilon\,\sigma_\pi(\varepsilon)\xi(\varepsilon)\varepsilon\int_{\varepsilon/2\gamma_p}^{\infty}dx\,x^{-2}n_{ph}(x,t), \quad (42)$$

(Waxman & Bahcall 1997) where $\sigma_\pi(\varepsilon)$ is the cross section for pion production for a photon with energy ε in the proton rest frame, $\xi(\varepsilon)$ is the average fraction of energy lost to the pion, and $\varepsilon_0=0.15$ GeV is the threshold energy. For a flat photon spectrum [$\varepsilon^2 n_{ph}(\varepsilon)\propto\varepsilon^\alpha$ with $\alpha\simeq 0$], the contribution to the first integral of equation (42) from photons at the Δ-resonance is comparable to that of photons of higher energy; thus

$$t_\pi^{-1}(\gamma_p,t)=\frac{c}{\gamma_p^2}\Delta\varepsilon\sigma_{\rm peak}\xi_{\rm peak}\varepsilon_{\rm peak}\int_{\varepsilon_{\rm peak}/2\gamma_p}^{\infty}dx\,x^{-2}n_{\rm ph}(x,t), \quad (43)$$

where $\sigma_{\rm peak}\simeq 5\times10^{-28}$ cm^2 and $\xi_{\rm peak}\simeq 0.2$ at the resonance $\varepsilon=\varepsilon_{\rm peak}=0.3$ GeV, and $\Delta\varepsilon\simeq 0.2$ is the peak width.

The rate of proton energy transfer to pions is given by

$$P_\pi(\gamma,t)=t_\pi^{-1}(\gamma_p,t)\gamma_p m_pc^2. \quad (44)$$

The energy loss rate of protons is calculated by numerical integration of the integral in equation (43). This calculation is carried out only in those cases where the Δ-resonance approximation is valid and can easily be extended to any photon spectrum by explicit integration of the integrals in equation (42). Roughly half of this energy is converted into high-energy photons through the π^0 decay. Each of the created photons carry 10% of the initial proton energy; thus the photon production rate is given by

$$R_\pi(\varepsilon=\gamma_pm_pc^2/10,\ t)=5t_\pi^{-1}(\gamma_p,\ t)n_p(\gamma_p,\ t), \quad (45)$$

where $n_p(\gamma_p)$ is the number density of protons at energy $\gamma_pm_pc^2$. Half of the energy lost by protons is converted into π^+, which decay into positron and neutrinos, $\pi^+\rightarrow\mu^++\nu_\mu\rightarrow e^++\nu_e+\bar{\nu}_\mu+\nu_\mu$. The energy of the π^+ is roughly evenly distributed between the decay products; thus the positron carries 5% of the initial proton energy, and the positron production rate is given by

$$Q_\pi\left[\gamma=\gamma_p(m_p/m_e)/20,\ t\right]=2.5t_\pi^{-1}(\gamma_p,t)n_p(\gamma_p,t). \quad (46)$$

Equations (45) and (46) provide only a crude approximation to the spectrum of high-energy photons and positrons produced by pion decay. However, photons and positrons that are created by pion decay are typically very energetic and participate in the high-energy electromagnetic cascade. Since the energy of these particles and photons is spread among the cascade products, and the final cascade spectrum has only weak dependence on the initial spectrum, it is appropriate to use the approximate expressions in equations (45) and (46).

3. NUMERICAL APPROACH

Several integration methods are used in solving the kinetic equations. A simple, first-order difference scheme was found adequate, except when dealing with synchrotron self-absorption

and with the evolution of the rapid high-energy electromagnetic cascades. Synchrotron self-absorption calculations are carried using a Cranck-Nickolson second-order integration scheme (see Press et al. 1992).

The particle and photon distributions are discretized, spanning the energy range relevant to the problem. Note that in the problems involved, this energy range can extend over 20 decades (see § 4 below). Spectra of cyclosynchrotron emission (eqs. [12] and [13]), Compton scattering (eqs. [19] and [27]), and pair production (eq. [28]) are precalculated and stored in tables.

Following simultaneously the evolution of the rapid high-energy electromagnetic cascade and the much slower evolution of low-energy processes is difficult. The "stationary" approximation used in previous works in treating the evolution of high-energy particles (see, e.g., Fabian et al. 1986; Lightman & Zdziarski 1987; Coppi 1992) cannot be used, due to the nonlinear nature of the cascade: as an energetic particle loses its energy, many secondaries are created, which, in turn, serve as primaries for further development of the cascade. As the cascade evolution is powered by inverse Compton scattering and pair production and annihilation, the injection rate of energetic photons and pairs depends on the entire particle and photon spectra.

Therefore, in treating this problem, a fixed time step is chosen, typically $10^{-4.5}$ times the dynamical time. Numerical integration is carried out with this fixed time step. At each time step, the cascade evolution is followed directly. Direct numerical integration is carried out only for the electrons, positrons, and photons for which the energy loss time or annihilation time is longer than the fixed time step. Electrons, positrons, and photons for which the energy loss time or annihilation time is shorter than the fixed time step are assumed to lose all their energy in a single time step, producing secondaries. The secondaries' spectra are determined by the spectra of the various physical processes, as presented in § 2, and by the relative rates of these processes. We discriminate between high-energy secondaries, which are secondaries for which the energy loss time or annihilation time are shorter than the fixed time step, and low-energy secondaries, which lose their energy or annihilate on a timescale longer than the fixed time step. The calculation is repeated for the high-energy secondaries, which are treated as a source of lower energy particles, until all the cascade energy is transferred to low-energy particles. Since in each step of the cascade calculation part of the energy is transferred into low-energy particles that do not participate in the cascade, convergence is guaranteed. In order to check for convergence of this method, we repeat the complete calculation with a shorter time step.

The time derivative of particle distributions due to synchrotron emission and Compton scattering is calculated by solving the continuity equation $\partial n(\gamma, t)/\partial t = \partial j(\gamma, t)/\partial E$, where $j(\gamma, t) \equiv n(\gamma, t)P(\gamma)$, and $P(\gamma)$ is the emitted power (see eq. [1]). In solving this equation, a flux limiter is used to ensure convergence for large time steps, and Neumann boundary conditions for the flux $j(\gamma, t)$ at the boundary points are used. The rate of change of particle distributions due to pair production and annihilation are calculated using equations (28) and (39). Conservation of particle number and energy is forced using the Lagrange multiplier method. This method was found to allow faster convergence (larger time steps).

At the low end of the particle spectrum, electrons and positrons gain energy via direct Compton scattering, on a timescale shorter than the fixed time step. In parallel to gaining energy, these particles lose energy via synchrotron emission on a much longer timescale, thus providing another challenge to numerical integration. Defining "very low energy particles" as particles that gain energy on a timescale shorter than the fixed time step, we treat this problem in the following way. At each time step, calculation of the number density of these particle is repeated iteratively until the particle distribution converges and the total emissivity equals the absorption. At each of the iteration steps, the calculated emissivity and absorption are stored and used in the calculation of the photon emission from these particles. Convergence of this method as well is checked by repeating the calculation with smaller time steps.

4. EXAMPLES OF NUMERICAL RESULTS

We give below several examples of the results of numerical calculations of GRB prompt emission spectra. Detailed descriptions of numerical results of prompt emission spectra and early afterglow emission spectra are found in Pe'er & Waxman (2004b, 2004c). Our calculations are done in the framework of the fireball model (see, e.g., Piran 2000; Mészáros 2002; Waxman 2003), in which the emission results from electron acceleration to ultrarelativistic energies by internal shocks within an expanding wind.

4.1. *Basic Assumptions, Plasma Conditions, and Particle Acceleration*

We calculate the emergent spectra following a single collision between two plasma shells. Denoting by Γ the characteristic wind Lorentz factor and assuming variation $\Delta\Gamma/\Gamma \sim 1$ on a timescale Δt, two shells collide at radius $r_i = 2\Gamma^2 c\Delta t$. For $\Delta\Gamma/\Gamma \sim 1$, two mildly relativistic ($\Gamma_s - 1 \sim 1$ in the wind frame) shocks are formed, one propagating forward into the slower shell ahead, and one propagating backward (in the wind frame) into the faster shell behind. The comoving shell width, measured in the shell rest frame, is $\Delta R = \Gamma c\Delta t$, and the comoving dynamical time, the characteristic time for shock crossing and shell expansion measured in the shell rest frame, is $t_{\rm dyn} = \Gamma\Delta t$. The shock waves, which propagate at relativistic velocity $v_s \sim c$ in the plasma rest frame, dissipate the plasma kinetic energy and accelerate particles to high energies. Since the shock velocity is time-independent during $t_{\rm dyn}$, the shock-heated comoving plasma volume is assumed to increase linearly with time; i.e., constant particle number density is assumed.

Under these assumptions, the shocked plasma conditions are determined by six free parameters. Three are related to the underlying source: the total luminosity $L = 10^{52}L_{52}$ ergs s^{-1}, the Lorentz factor of the shocked plasma, $\Gamma = 10^{2.5}\Gamma_{2.5}$, and the variability time $\Delta t = 10^{-4}\Delta t_{-4}$ s. Three additional parameters are related to the collisionless-shock microphysics: the fraction of postshock thermal energy carried by electrons, $\epsilon_e = 10^{-0.5}\epsilon_{e,0.5}$, and by magnetic field, $\epsilon_B = 10^{-0.5}\epsilon_{B,0.5}$, and the power-law index of the accelerated electrons' Lorentz factor distribution, $d\log n_e/d\log\gamma = -p$, assumed to extend over the range $\gamma_{\rm min} \le \gamma \le \gamma_{\rm max}$.

The comoving proton number density is

$$n_p \approx \frac{L}{4\pi r_i^2 c\Gamma^2 m_p c^2} = 6.7\times10^{14}L_{52}\Gamma_{2.5}^{-6}\Delta t_{-4}^{-2}\ {\rm cm}^{-3}. \quad (47)$$

The internal energy density is $u_{\rm int} = L/(4\pi r_i^2 c\Gamma^2)$, resulting in a magnetic field

$$B = \sqrt{\frac{\epsilon_B L}{2\Gamma^6 c^2\Delta t^2}} = 2.9\times10^6 L_{52}^{1/2}\epsilon_{B,-0.5}^{1/2}\Gamma_{2.5}^{-3}\Delta t_{-4}^{-1}\ {\rm G}. \quad (48)$$

4.1.1. *Particle Acceleration*

Since the details of the acceleration mechanism are not yet known, we adopt the common assumption of a power-law energy distribution of the accelerated electrons Lorentz factor γ. The power-law index p of the accelerated particles is a free parameter of the model. The maximum Lorentz factor of the accelerated electrons, $\gamma_{\rm max}$, is obtained by equating the acceleration time, $t_{\rm acc} = \gamma m_e c^2/cqB$, and the synchrotron cooling time, $t_{\rm syn} = 9m_e^3c^5/4q^4B^2\gamma$, to obtain $\gamma_{\rm max} = (6\pi q/\sigma_{\rm T}B)^{1/2}$. The accelerated particles assume a power-law energy distribution above a minimum Lorentz factor $\gamma_{\rm min}$, which is obtained by simultaneously solving

$$n_e = \int_{\gamma_{\rm min}}^{\gamma_{\rm max}} \frac{dn_e}{d\varepsilon} d\varepsilon, \quad u_e = \int_{\gamma_{\rm min}}^{\gamma_{\rm max}} \varepsilon \frac{dn_e}{d\varepsilon} d\varepsilon, \tag{49}$$

where n_e and $u_e \equiv \epsilon_e u_{\rm int}$ are the number and energy densities of the electrons. The injected particle distribution below $\gamma_{\rm min}$ is assumed thermal with temperature $\theta \equiv kT/m_ec^2 = 3\gamma_{\rm min}$, and exponential cutoff is assumed above $\gamma_{\rm max}$. In the results shown below, no proton acceleration is assumed.

Our calculations are carried in the plasma (comoving) frame. The particle distributions are discretized, spanning a total of 10 decades of energy ($\gamma\beta_{\rm min} = 10^{-3}$ to $\gamma\beta_{\rm max} = 10^7$). The photon bins span 14 decades of energy, from $\alpha_{\rm min} \equiv \varepsilon_{\rm min}/m_ec^2 = 10^{-8}$ to $\alpha_{\rm max} \equiv \varepsilon_{\rm max}/m_ec^2 = 10^6$. No a priori photon field is assumed.

4.2. *Low Compactness*

We examined the dependence of the emergent spectrum on the uncertain values of the free parameters of the model. We found that the spectral shape strongly depends on the dimensionless compactness parameter l, defined by $l \equiv L\sigma_{\rm T}/Rm_ec^3$, where L is the luminosity and R is a characteristic length of the object. For low value of the comoving compactness, $l' \lesssim 10$, the optical depth to pair production and to scattering by pairs is smaller than 1 (Pe'er & Waxman 2004b); thus the synchrotron-SSC emission model provides a fairly good approximation of the resulting spectrum. Therefore, before applying our model to examine a realistic scenario (i.e., comparison with observations), we first compare our numerical results to the analytical model predictions in the parameter-space region where the latter are valid. Figure 1 presents numerical results in this case, where a power-law index $p = 3$ was used to allow the synchrotron and Compton peaks to be distinctively apparent.

The synchrotron peak presented in Figure 1 at $\varepsilon_{\rm peak}^{\rm obs} \simeq 10$ keV is in excellent agreement with the analytical results of the optically thin synchrotron model prediction,

$$\varepsilon_{\rm peak}^{\rm obs} = \hbar \frac{3}{2}\frac{qB}{m_ec}\gamma_{\rm min}^2\Gamma = 1.4\times10^4 L_{52}^{1/2}\epsilon_{e,-0.5}^2\epsilon_{B,-0.5}^{1/2}\Gamma_{2.5}^{-2}\Delta t_{-2}^{-1}\ {\rm eV}, \tag{50}$$

where $\gamma_{\rm min} \simeq \epsilon_e(m_p/m_e)(p-2)/(p-1)$ was used. The Lorentz factor of the electrons that cool on a timescale that is equal to the dynamical timescale is $\gamma_c \sim 1$; thus above $\varepsilon_{\rm peak}$ the spectral index $\nu F_\nu \propto \nu^\alpha$ is $\alpha = 1 - p/2 = -1/2$, while below $\varepsilon_{\rm peak}$, $\alpha = 1/2$. The self-absorption frequency, $\varepsilon_{\rm ssa}^{\rm obs} \simeq 100$ eV, is somewhat lower than the self-absorption frequency predicted for a pure power-law distribution of the electrons,

$$\varepsilon_{\rm ssa}^{\rm obs} = 600 L_{52}^{2/3}\epsilon_{e,-0.5}^{1/3}\epsilon_{B,-0.5}^{1/3}\Gamma_{2.5}^{-8/3}\Delta t_{-2}^{-1}\ {\rm eV}, \tag{51}$$

where a power-law index $p = 2$ for particles below $\gamma_{\rm min}$ is assumed. This discrepancy is due to the fact that the low-energy particles are not power-law distributed, but have a quasi-Maxwellian distribution due to photon reabsorption (see Fig. 2).

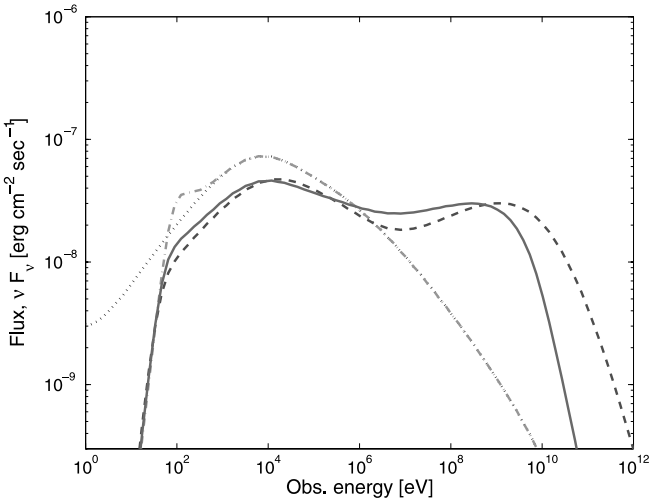

FIG. 1.—Time-averaged GRB prompt emission spectra obtained after a two-shell collision, characterized by a low compactness parameter. Results are shown for $L = 10^{52}$ ergs, $\epsilon_e = \epsilon_B = 10^{-0.5}$, $p = 3$, $\Delta t = 10^{-2}$ s, and $\Gamma = 300$. The comoving compactness parameter is $l' = 2.5$. *Dotted curve*: Cyclosynchrotron emission only. *Dash-dotted curve*: Synchrotron emission and self-absorption only. *Dashed curve*: Synchrotron emission, synchrotron self-absorption, and Compton scattering. *Solid curve*: All processes included, including pair production and annihilation, but excluding proton acceleration. Luminosity distance $d_L = 2\times10^{28}$ and $z = 1$ were assumed. [*See the electronic edition of the Journal for a color version of this figure.*]

Without pair production, the SSC model predictions of the Compton scattering peak at $\varepsilon_{\rm IC,peak}^{\rm obs} = \gamma_{\rm min}^2\varepsilon_{\rm peak}^{\rm obs} = 1.3$ GeV agrees well with the numerical result, $\varepsilon_{\rm IC,peak}^{\rm obs} = 1.5$ GeV. The 1 GeV flux is comparable to the flux at 10 keV, as predicted by analytic calculations based on the Compton y parameter, $y = 1$ in the scenario presented in Figure 1.

Pair production causes a cutoff at high energies. For a flat spectrum, $\varepsilon^2 n_{\rm ph}(\varepsilon) \propto \varepsilon^0$ (which is a good approximation provided that ϵ_B is not much below equipartition), the optical depth to pair production is well approximated by

$$\tau_{\gamma\gamma}(\varepsilon) = \Delta R n_{\rm ph}(\varepsilon)\frac{3}{16}\sigma_{\rm T} = \Gamma c\Delta t\frac{U_{\rm ph}}{\log(\varepsilon_{\rm max}/\varepsilon_{\rm peak})}\frac{\varepsilon}{(m_ec^2)^2}\frac{3}{16}\sigma_{\rm T} \tag{52}$$

and is larger than unity at

$$\tilde{\varepsilon}_\tau^{\rm obs} \geq 3\times10^8\log\left(\frac{\varepsilon_{\rm max}}{\varepsilon_{\rm peak}}\right)L_{52}^{-1}\epsilon_{e,-0.5}^{-1}\Gamma_{2.5}^6\Delta t_{-2}\ {\rm eV}, \tag{53}$$

in an excellent agreement with the numerical results. Here $U_{\rm ph}$ is the photon energy density, given by $U_{\rm ph} \approx \epsilon_e L/4\pi r_i^2 c\Gamma^2$. For this value of the compactness, pair annihilation does not play a significant role, while scattering by the created pairs flattens the spectrum at 10 keV to 1 GeV.

Even though the analytic approximation is in fairly good agreement with the numerical calculations, there are important discrepancies between the analytic approximation and the numerical calculation. The electron distribution shows a peak at $\gamma \sim 1.05$ ($\beta \sim 0.3$), resulting in a deviation of the self-absorption frequency from the analytic calculation. These electrons affect the high-energy spectrum by Compton scattering, resulting in a

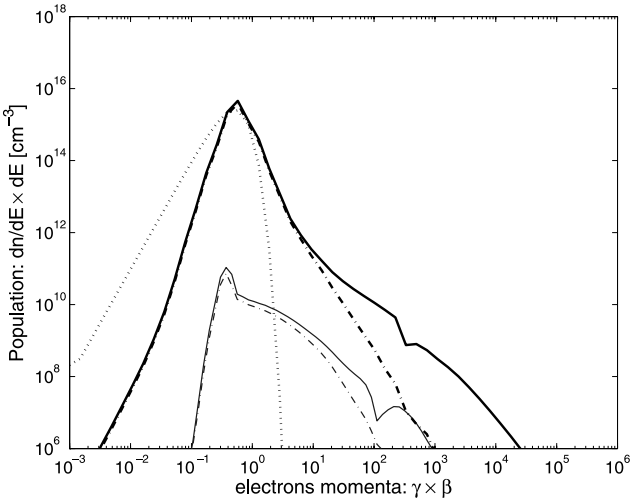

FIG. 2.—Particle distribution at the end of the dynamical time. *Thick curves*: $\Delta t = 10^{-4}$ s, $l' = 250$. *Thin curves*: $\Delta t = 10^{-2}$ s, $l' = 2.5$. All other parameters are the same as in Fig. 1. *Solid curves*: Electron distribution. *Dash-dotted curve*: Positron distribution. The dotted line shows a Maxwellian distribution at temperature $\theta \equiv kT/m_e c^2 = 0.08$. [*See the electronic edition of the Journal for a color version of this figure.*]

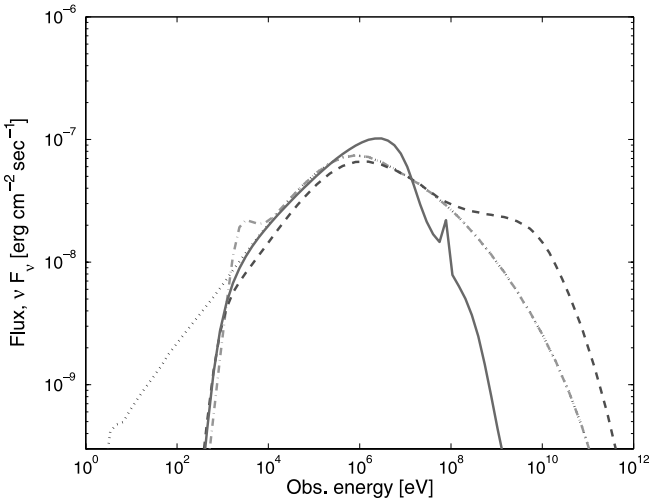

FIG. 3.—Time-averaged GRB prompt emission spectra obtained after a two-shell collision, characterized by a high compactness parameter (not corrected for the high optical depth to Thomson scattering). Results are shown for $L = 10^{52}$ ergs, $\epsilon_e = \epsilon_B = 10^{-0.5}$, $p = 3$, $\Delta t = 10^{-4}$ s, and $\Gamma = 300$. The comoving compactness parameter is $l' = 250$. *Dotted curve*: Cyclosynchrotron emission only. *Dash-dotted curve*: Synchrotron emission and self-absorption only. *Dashed curve*: Synchrotron emission, synchrotron self-absorption, and Compton scattering. *Solid curve*: All processes included, including pair production and annihilation, but excluding proton acceleration. Luminosity distance $d_L = 2 \times 10^{28}$ and $z = 1$ were assumed. [*See the electronic edition of the Journal for a color version of this figure.*]

nearly flat ($\alpha \sim 0$) spectrum above 10 keV. We showed (Pe'er & Waxman 2004b) that the spectrum is nearly independent of the power-law index of the accelerated electrons, p.

4.3. *High Compactness*

Figure 3 shows an example of our numerical results for large comoving compactness, $l' = 250$. At large values of the compactness parameter, $l' > 30$, the synchrotron-SSC model predictions do not provide an appropriate description of the spectrum. Therefore, the numerical results may provide some insight on the inconsistency between some of the observations and the analytical predictions, as mentioned in § 1.

In the scenario of large compactness, Compton scattering by pairs becomes the dominant emission mechanism. Both electrons and positrons lose their energy much faster than the dynamical time, and a quasi-Maxwellian distribution with an effective temperature $\theta \equiv kT/m_e c^2 \simeq 0.05-0.1$ is formed. Photons upscattered by the pairs create the peak at $\Gamma\theta m_e c^2 \sim 5$ MeV. The results shown in Figure 3 are not corrected for the fact that the optical depth to scattering by pairs is large, $\tau_\pm \sim 10$ (see § 2). Therefore, the emergent spectral peak is expect to be at lower energy, at $\sim$1 MeV (for detailed discussion see Pe'er & Waxman 2004b). The moderate Compton y parameter, $y \simeq 4\theta\tau \approx 4\theta_{-1}\tau_1$, results in a spectral slope $\nu F_\nu \propto \nu^\alpha$ with $\alpha \approx 0.5$ between $\varepsilon_{\rm ssa} \approx 3$ keV and $\varepsilon_{\rm peak} \approx 5$ MeV. The peak at $\Gamma m_e c^2 \sim 10^2 \Gamma_{2.5}$ MeV is formed by pair annihilation. The self-absorption frequency, $\varepsilon_{\rm ssa} \simeq 3$ keV, is well below the prediction for a power-law index $p = 2$ of particles below $\gamma_{\rm min}$. This is attributed to the quasi-Maxwellian distribution of particles at low energies (see Fig. 2). The inverse Compton peak flux is lower than the synchrotron peak flux, due to the Klein-Nishina suppression at high energies.

Even though the results presented here are for illustrative purposes only and are not aimed at explaining a particular observation, we note that the obtained numerical results are is agreement with some of the observations that were found to be inconsistent with the optically thin synchrotron–SSC model predictions. Examples are the steep slopes observed at low energies (Preece et al. 1998; Frontera et al. 2000; Ghirlanda et al. 2003) and the steep slopes above $\varepsilon_{\rm peak}^{\rm obs}$ obtained by Baring & Braby (2004). Further results of our study are presented in Pe'er & Waxman (2004b). Comparison of the numerical results with the high-energy component reported by González et al. (2003) is presented in Pe'er & Waxman (2004a).

5. SUMMARY AND DISCUSSION

We have described a time-dependent numerical model that calculates emission of radiation from relativistic plasma composed of homogeneous and isotropic distributions of electrons, positrons, protons, and photons and permeated by a time-independent magnetic field. We assume the existence of a dissipation process that produces energetic particles at constant rates. The particles interact via cyclosynchrotron emission, synchrotron self-absorption, inverse and direct Compton scattering, $e^\pm$ pair production and annihilation, and photomeson interactions that produce energetic photons and positrons following the decay of energetic pions. Exact cross sections valid at all energies, including the Klein-Nishina suppression at high energies, are used in describing the physical processes. Exact spectra are used in describing cyclosynchrotron emission, synchrotron self-absorption, Compton scattering, and pair production, and approximate spectra are used in the description of pair annihilation.

We explained in § 3 our unique integration method, which overcomes the challenge of the many orders of magnitude difference in characteristic timescales. We presented the various integration techniques used for solving the kinetic equations describing the evolution of particle and photon distributions at all energy scales. By following directly the development of the rapid high-energy electromagnetic cascades at each time step, we obtain the spectrum at high energies, up to $\geq$100 TeV. Our method enables to follow the development of the spectrum created in the parameter-space region of large compactness, where no analytic approximation is valid. This method also improves over previous ones by providing a more accurate

treatment of photon emission and absorption in the presence of magnetic fields.

We have given several examples of numerical calculations in § 4. In parameter-space regions where analytical approximations are valid, our numerical results are in good agreement with analytic results. We have pointed out some significant discrepancies between the analytical approximations and the numerical calculation, and explained their origin. We presented examples of new results for parameter-space regions where analytic approximations are not valid. We pointed out that our results are consistent with numerous observations, including observations that are inconsistent with the optically thin synchrotron–SSC model predictions. Further results of our study of GRB prompt emission and early afterglow emission can be found in Pe'er & Waxman (2004b, 2004c).

The next generation high-energy detectors, such as the *SWIFT* and *GLAST* satellites, and the sub-TeV ground-based Cerenkov detectors, such as MAGIC, HESS, VERITAS, and CANGAROO III,[3] are expected to increase the GRB prompt emission and early afterglow emission detection rate by an order of magnitude, to allow detection of >GeV emission from GRBs, and to detect the high-energy spectra of thousands of AGNs at various distances. Thus, detailed numerical models that are capable of producing accurate spectra over a wide energy scale are necessary for analyzing and understanding the experimental data.

This research was supported in part by ISF and Minerva grants.

[3] See http://www.swift.psu.edu, http://www-glast.stanford.edu, http://wwwmagic.mppmu.mpg.de, http://www.mpi-hd.mpg.de/hfm/HESS/HESS.html, http://veritas.sao.arizona.edu, and http://icrhp9.icrr.u-tokyo.ac.jp, respectively.

APPENDIX

COULOMB SCATTERING

In the limit of relativistic particle scattering off cool thermal pair distribution ($\theta \ll 1$, $\gamma \gg 1$), the energy loss rate of the relativistic particle can be approximated by $d\gamma/dt \approx -3/2\sigma_{\rm T} c n_{\pm} \ln\Lambda$, or $t_{ee}^{-1} \equiv -(1/\gamma)d\gamma/dt \approx 4\pi c r_0^2 n_{\pm}\gamma^{-1} \ln\Lambda$ (Gould 1975), where $n_{\pm}$ is the number density of the thermal pairs. The relevant value of the Coulomb logarithm Λ is $\Lambda \approx \gamma^{1/2} m_e c^2/h\omega_p$, where $\omega_p = (4\pi n_{\pm} e^2/m_e)^{1/2}$ is the plasma frequency.

Assuming that the pairs' energy distribution is thermal, that their number density is $n_{\pm} \equiv f n_p$, where n_p is the proton number density, and that $n_p \approx u_{\rm int}/m_p c^2$, where $u_{\rm int}$ is the internal energy density, comparing the Coulomb cooling time and the synchrotron cooling time, $t_{\rm syn} = 9m_e^3 c^5/4q^4 B^2\gamma$, using $B^2 = 8\pi\epsilon_B u_{\rm int}$, gives

$$\frac{t_{\rm syn}}{t_{ee}} = \frac{9}{8}\frac{m_e}{m_p}\frac{f\ln\Lambda}{\epsilon_B\gamma^2} \simeq \frac{1}{3\gamma^2} f_1 \epsilon_{B,-0.5}^{-1}, \tag{A1}$$

where typical values $f = 10 f_1$ and $\ln\Lambda \approx 20$ are assumed. It is therefore concluded that for relativistic electrons and for magnetic field not many orders of magnitude below equipartition, electrons lose their energy by synchrotron emission on a timescale much shorter than the energy loss time by Coulomb scattering. A more accurate approximation of t_{ee} (Haug 1988; Coppi & Blandford 1990) does not change this result.

REFERENCES

Band, D., et al. 1993, ApJ, 413, 281
Baring, M. G., & Braby, M. L. 2004, ApJ, 613, 460
Bekefi, G. 1966, Radiation Processes in Plasmas (New York: Wiley)
Blumenthal, G. R., & Gould, R. J. 1970, Rev. Mod. Phys., 42, 237
Bonometto, S., & Rees, M. J. 1971, MNRAS, 152, 21
Bötcher, M., & Schlickeiser, R. 1997, A&A, 325, 866
Burns, M. L., & Lovelace, R. V. E. 1982, ApJ, 262, 87
Coppi, P. S. 1992, MNRAS, 258, 657
Coppi, P. S., & Blandford, R. D. 1990, MNRAS, 245, 453
Fabian, A. C., Blandford, R. D., Guilbert, P. W., Phinney, E. S., & Cuellar, L. 1986, MNRAS, 221, 931
Frontera, F., et al. 2000, ApJS, 127, 59
Ghirlanda, G., Celotti, A., & Ghisellini, G. 2003, A&A, 406, 879
Ghisellini, G., Guilbert, P. W., & Svensson, R. 1988, ApJ, 334, L5
Ginzburg, V. L., & Syrovatskii, S. I. 1965, ARA&A, 3, 297
———. 1969, ARA&A, 7, 375
González, M. M., et al. 2003, Nature, 424, 749
Gould, R. J. 1975, ApJ, 196, 689
Gould, R. J., & Schréder, G. P. 1967, Phys. Rev., 155, 1404
Gruzinov, A., & Waxman, E. 1999, ApJ, 511, 852
Guilbert, P. W., Fabian, A. C., & Rees, M. J. 1983, MNRAS, 205, 593
Haug, E. 1988, A&A, 191, 181
Jones, F. C. 1968, Phys. Rev., 167, 1159
Lang, K. R. 1999, Astrophysical Formulae (Berlin: Springer)
Lightman, A. P., & Zdziarski, A. A. 1987, ApJ, 319, 643
Mahadevan, R., Narayan, R., & Yi, I. 1996, ApJ, 465, 327
McCray, R. 1969, ApJ, 156, 329
Mészáros, P. 2002, ARA&A, 40, 137
Mészáros, P., & Rees, M. J. 1997, ApJ, 476, 232
Paczyński, B., & Rhoads, J. E. 1993, ApJ, 418, L5
Panaitescu, A., & Mészáros, P. 1998, ApJ, 501, 772
Pe'er, A., & Waxman, E. 2004a, ApJ, 603, L1
———. 2004b, ApJ, 613, 448
———. 2004c, ApJ, submitted (astro-ph/0407084)
Pilla, R. P., & Loeb, A. 1998, ApJ, 494, L167
Piran, T. 2000, Phys. Rep., 333, 529
Preece, R. D., et al. 1998, ApJ, 506, L23
———. 2002, ApJ, 581, 1248
Press, W. H., Flannery, B. P., Teukolsky, S. A., & Vetterling, W. T. 1992, Numerical Recipes in C: The Art of Scientific Computing (Cambridge: Cambridge Univ. Press)
Rybicki, G. B., & Lightman, A. P. 1979, Radiative Processes in Astrophysics (New York: Wiley)
Sari, R., Piran, T., & Narayan, R. 1998, ApJ, 497, L17
Svensson, R. 1982, ApJ, 258, 321
———. 1987, MNRAS, 227, 403
Vietri, M. 1997, ApJ, 478, L9
Waxman, E. 2003, in Supernovae and Gamma-Ray Bursts, ed. K. Weiler (Berlin: Springer), 393
Waxman, E., & Bahcall, J. 1997, Phys. Rev. Lett., 78, 2292
Zdziarski, A. A., & Lightman, A. P. 1985, ApJ, 294, L79